Ratiometric Flapping Force Probe That Works in Polymer Gels

AUTHOR(S):

Yamakado, Takuya; Saito, Shohei

CITATION:

Yamakado, Takuya ...[et al]. Ratiometric Flapping Force Probe That Works in Polymer Gels. Journal of the American Chemical Society 2022, 144(6): 2804-2815

ISSUE DATE:

2022-02-16

URL:

http://hdl.handle.net/2433/276811

JACS
JOURNAL OF THE AMERICAN CHEMICAL SOCIETY
pubs.acs.org/JACS
Article

Ratiometric Flapping Force Probe That Works in Polymer Gels

Takuya Yamakado and Shohei Saito*

Cite This: J. Am. Chem. Soc. 2022, 144, 2804−2815
Read Online
ACCESS | Metrics & More | Article Recommendations | Supporting Information

ABSTRACT: Polymer gels have recently attracted attention for their application in flexible devices, where mechanically robust gels are required. While there are many strategies to produce tough gels by suppressing nanoscale stress concentration on specific polymer chains, it is still challenging to directly verify the toughening mechanism at the molecular level. To solve this problem, the use of the flapping molecular force probe (FLAP) is promising because it can evaluate the nanoscale forces transmitted in the polymer chain network by ratiometric analysis of a stress-dependent dual fluorescence. A flexible conformational change of FLAP enables real-time and reversible responses to the nanoscale forces at the low force threshold, which is suitable for quantifying the percentage of the stressed polymer chains before structural damage. However, the previously reported FLAP only showed a negligible response in solvated environments because undesirable spontaneous planarization occurs in the excited state, even without mechanical force. Here, we have developed a new ratiometric force probe that functions in common organogels. Replacement of the anthraceneimide units in the flapping wings with pyreneimide units largely suppresses the excited-state planarization, leading to the force probe function under wet conditions. The FLAP-doped polyurethane organogel reversibly shows a dual-fluorescence response under sub-MPa compression. Moreover, the structurally modified FLAP is also advantageous in the wide dynamic range of its fluorescence response in solvent-free elastomers, enabling clearer ratiometric fluorescence imaging of the molecular-level stress concentration during crack growth in a stretched polyurethane film.

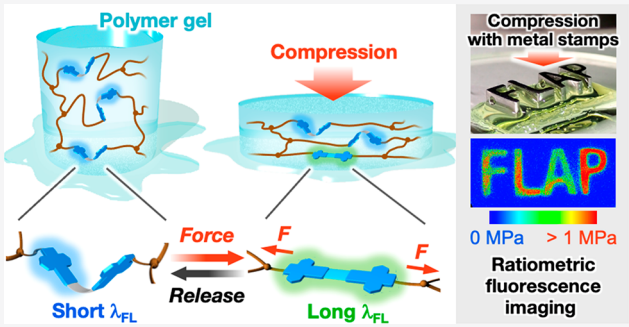

INTRODUCTION

A polymer gel is composed of a polymer chain network swollen with a solvent. Hydrogels have been widely used for drug delivery systems[1] and biocompatible materials[2] due to their high solvent retention properties and flexibility. In addition to these classical applications, mechanically robust gels have been increasingly studied for use in wearable electronics,[3] actuators,[4] soft robotics,[5] and mechanoactive materials.[6]

However, polymer gels are inherently fragile because of their low volume fraction of polymer chains and inhomogeneous network structure.[7] To make tough polymer gels, many strategies have been proposed in recent decades,[8,9] including the motifs of double network structures,[10−13] noncovalent crosslinks,[14−18] nanoparticles,[19−22] and crystalline structures.[23,24] These materials have been designed to dissipate the energy of mechanical stress concentrated on specific polymer chains,[25] as it has also been reported for elastomers.[26−31] Furthermore, to overcome the inhomogeneity of polymer networks, unique polymer networks have been studied based on (1) multiarm macromers with uniform chain length[32−35] and (2) polymer gels with rotaxane-based slidable cross-links.[24,36−38] These nanoscopic polymer designs are intrinsically important for the creation of polymer gels with remarkable mechanical properties. However, it remains challenging to directly elucidate the toughening mechanism at the nanoscale.[39]

Notably, polymer mechanochemistry has rapidly developed as a related area.[40,41] A variety of mechanophores exhibit color changes[42−53] and/or luminescence responses[26,54−61] when a relatively weak covalent bond undergoes the intramolecular cleavage by mechanical stimuli, as represented by spiropyran. While these mechanophores are widely used for developing mechanoresponsive materials,[62−65] they can also be used as "force probes" to evaluate molecular-level forces transmitted in a polymer chain network, as long as the chemical doping of the mechanophore does not have a significant influence on the intrinsic mechanical properties of host polymers.[66,67] Recently, several applications of force probes for quantitative mapping of the local stress distribution in multinetwork elastomers during the crack propagation have been reported.[68−71] In these reports, the important role of the sacrificial bonds in the toughening mechanism of topological polymers has been

Received: December 9, 2021
Published: February 2, 2022

https://doi.org/10.1021/jacs.1c12955
J. Am. Chem. Soc. 2022, 144, 2804−2815

demonstrated. Mechanoresponsive system with a reversible response is more useful,[72−83] which would enable real-time monitoring of local force distribution in the elastic polymer deformation.

FRET pairs would be an alternative tool to probe small forces generated before the covalent bond scission, while at least 200 piconewtons (pN) are required for the intramolecular bond cleavage of spiropyran.[43,45] The FRET pairs are commonly used in mechanobiology.[84−87] Supramolecular structural changes, such as the unravelling of a DNA linker,[88,89] induce a fluorescence (FL) response via perturbation of the FRET efficiency. The force threshold to cleave the hydrogen bonds in DNA/proteins has been estimated to be tens of piconewtons, which is 1 or 2 orders of magnitude lower than that of conventional mechanophores;[84−89] however, the FRET efficiency is sensitive to multiple parameters, such as the distance between and the relative orientation[90] of the two dyes, and the chromophores themselves are not mechanoresponsive.

Flapping molecules (FLAP) constitute another category of conformationally flexible force probes,[91] which are unique due to their single-component dual FL properties that originate from their interchangeable bent and planar conformations.[92,93] The force threshold of the single-molecule fluorescence switching of FLAP has been predicted by calculations to be approximately 100 pN.[91] The force range is below that for covalent bond scission (from 200 pN to several nN) and above thermal fluctuation (several pN). The molecular design of the central flexible hinge is not limited to cyclooctatetraene (COT); a series of *N*,*N*′-disubstituted-dihydrophenazines have also been reported as dual fluorescence flexible chromophores.[94−97] Figure 1 shows the newly synthesized

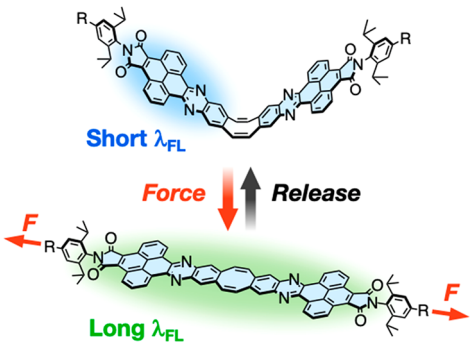

Figure 1. Conformational change of a structurally modified flapping force probe (FLAP) that enables a real-time ratiometric fluorescence analysis of the molecular-level stress concentration in polymer gels. λ_{FL}: Fluorescence wavelength.

FLAP in this study. Ratiometric force analysis using FLAP shows promise to obtain the high signal-to-noise ratio in a simple experimental setup by canceling out the effects of inhomogeneous probe concentration, excitation source variation, and light scattering by sample specimens. We recently reported a flapping force probe **FLAP0** bearing the anthraceneimide wings (Figure 2a and 2b).[91] In the narrow free volume of the solvent-free elastomers, **FLAP0** was surrounded by the polymer chains, suppressing the spontaneous planarization in the S_1 excited state. As a result, only the short λ_{FL} band of the bent form was observed in the steady-state FL spectrum of the unstretched **FLAP0**-doped film, while compulsory planarization in the S_0 ground state was induced by stretching the film, accompanied by the enhancement of the FL intensity ratio, I_{Long}/I_{Short} (Figure 2a and 2b). In the same previous report, the ratiometric FL analysis of the **FLAP0**-doped polyurethanes revealed that the local stress concentration is almost twice as biased at cross-linkers than at the main chains of the polymer network, particularly in the strain-hardening region.[91]

With these results in hand, we hypothesized that flapping force probes would also be useful for quantifying local stress concentration in gels, which are more fragile than elastomers (see the graphic in the abstract). However, **FLAP0** only showed a negligible FL response to mechanical stress in organogels, because the solvated **FLAP0** molecule underwent the spontaneous conformational planarization in the S_1 excited state, emitting a long λ_{FL} band even without mechanical stress (Figure 2c). To solve this problem, we have modified the molecular design of the FLAP force probe from the flapping anthraceneimide (**FLAP0**) to the flapping pyreneimide (**FLAP1**) (Figure 2b). This structural modification was expected to tune the excited-state energy profile by increasing the S_1 barrier, thus suppressing the S_1 planarization and allowing a mechanical response in polymer gels (Figure 2d). Namely, the distribution of the planar S_1 species of **FLAP1** became more populated only when the mechanical stress was applied. This structural modification into **FLAP1** also resulted in an improvement in the dynamic range of the stress-induced FL spectral change of the stretched elastomers (Figure 2b).

RESULTS AND DISCUSSION

Synthesis and Characterization of a New Force Probe. The molecular structure of a new force probe was designed based on the previously obtained insight. In a series of flapping acene dimers, we have reported that π-extension of the rigid wings of FLAP suppressed the spontaneous excited-state planarization.[98,99] Since this suppression is necessary for designing a force probe compatible with gels, we here selected a large π system for **FLAP1** among a variety of π-conjugated structures.[100] Pyrene-fused pyrazaacene[101,102] is suitable for this purpose, whose structure can be constructed by a reliable condensation reaction of pyrene dione and aromatic amines (Figure 3a). Briefly, a bulky 2,6-diisopropylphenyl group was introduced to prevent the aggregation of the fluorophore in solution or polymers. Reactions of the rigid wings, a pyrene dione derivative **3**, with the flexible COT joint, tetramine of dibenzo[*a*,*e*]cyclooctatetraene **4**[103] was conducted in a mixed solvent of chloroform and acetic acid under heating, providing **FLAP1-H** as a model compound of the force probe in 72% yield. **FLAP1-OH** was synthesized from **9**, in which the hydroxy groups were introduced at the R^1 position as a reactive group for polymerization. Note that mesityl groups (Mes) were attached to the R^2 position to improve solubility. **Wing1-H** and **Wing1-OH** (see Figure 4b and Section 2 in SI) were synthesized as reference compounds by the reaction of *o*-phenylenediamine with **3** or **9**.

To determine the structures of the prepared FLAP probes, single-crystal X-ray crystallography was conducted. While **Wing1-OH** readily formed crystals suitable for this analysis (Figure S3.2), the crystals of **FLAP1-OH** and **FLAP1-BC** (capped with the butylcarbamoyloxy groups at the probe termini) were not suitable for the measurement. We finally obtained the single-crystal X-ray structure of **FLAP1-OH′**, which possesses 3,5-di-*tert*-butylphenyl groups instead of the mesityl groups. As shown in Figure 3b, **FLAP1-OH′** exhibited a V-shaped structure in crystals, and the bending angles of the

https://doi.org/10.1021/jacs.1c12955
J. Am. Chem. Soc. 2022, 144, 2804−2815

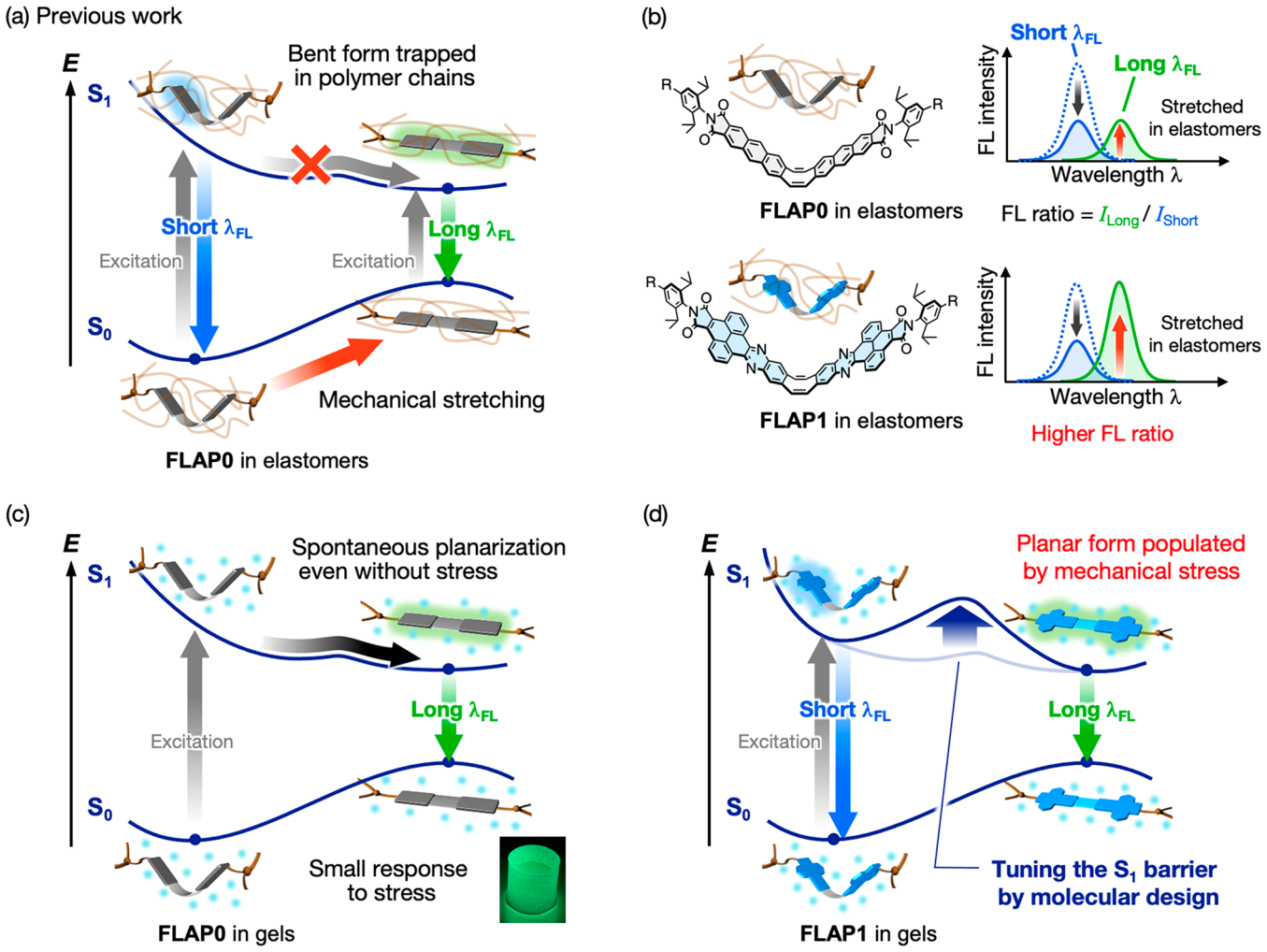

Figure 2. (a) Force probe function of **FLAP0** chemically doped into a solvent-free elastomer. (b) Chemical structures of **FLAP0** and **FLAP1** (left). Wider dynamic range of **FLAP1** (right) in the FL spectral response to mechanical stress in solvent-free elastomers (see the discussion in Figure 6). (c) S_0 and S_1 energy profiles of **FLAP0** in the presence of solvent molecules. A photograph of the **FLAP0**-doped organogel is shown in the inset. (d) Excited-state engineering of the S_1 energy profile under wet conditions by changing the molecular structure from **FLAP0** to **FLAP1**.

central cyclooctatetraene (COT), defined by the inset in Figure 5b, were 44.2° and 45.0°, which are comparable to those of the previously reported flapping molecules.[98,104]

Dual Fluorescence in Solution. The optical properties of **FLAP1-H** in toluene were measured to determine whether the excited-state planarization of the new force probe was adequately suppressed. As shown in Figure 4a, the absorption spectrum showed a maximum at 447 nm, and the FL spectrum showed a maximum at approximately 479 nm (corresponding to a small Stokes shift of 1720 cm^{-1}). On the other hand, the previously reported anthracene-based force probe (**FLAP0-H**) underwent spontaneous planarization in toluene and exhibited a FL spectrum with a peak at 525 nm, corresponding to a large Stokes shift (4800 cm^{-1}) (Figure 5a, inset).[93] This result suggests that **FLAP1-H** emitted FL mainly from the bent form due to the effective suppression of the excited-state planarization, as expected. The FL quantum yield of **FLAP1-H** was 0.44 in toluene. Importantly, **FLAP1-H** showed a small FL peak at 523 nm with a broad FL band at around 460−480 nm (green solid line in Figure 4a). The shape of the FL bands in the longer wavelength region was similar to that for **FLAP0-H** (Figure 5a, inset), in spite of their skeletal difference. When the FL spectrum of **FLAP1-H** was measured in a rigid PMMA matrix, in which the conformational planarization of FLAP is not allowed due to the confined space with a small free volume,[105] the peak at 523 nm disappeared (blue dotted line in Figure 4a). In contrast, no spectral change between toluene and PMMA was observed for **Wing1-H** (Figure 4b). Moreover, the FL lifetime of **FLAP1-H** can be fitted by two components (SI, Section 4.3). Together, these results suggest that the long-wavelength FL of **FLAP1-H** can be attributed to a partially populated planar form in the excited state.

To gain insight into the equilibrium between the bent and planar forms in the S_1 excited state, the variable-temperature FL spectra of **FLAP1-H** were measured in toluene. The relative FL intensity of the long-wavelength component decreased when the temperature was lower or higher than 233 K (Figures 4c and 4d). On the other hand, such behavior was not observed for **Wing1-H** (Figure S4.5). No concentration dependence was observed in the shape of the absorption and FL spectra (Figure S4.1), and no significant changes were observed in the variable-temperature excitation spectra of **FLAP1-H** (Figure S4.4), suggesting that no impurities present and no structural changes occurred in the ground state. The variable-temperature FL spectra in Figures 4c and 4d are typical of a dual FL system existing in

https://doi.org/10.1021/jacs.1c12955
J. Am. Chem. Soc. 2022, 144, 2804−2815

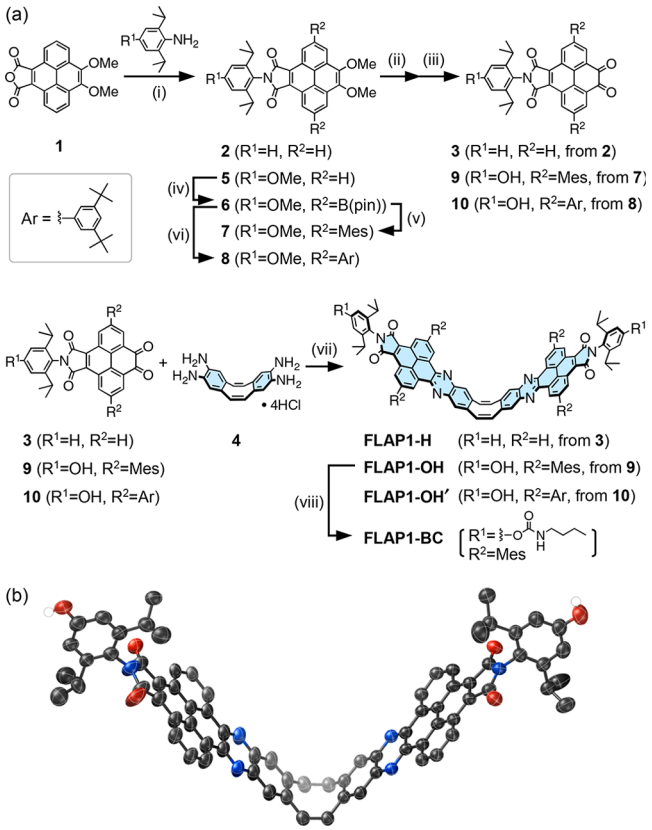

Figure 3. (a) Synthesis of the flapping pyreneimides. Mes: mesityl groups. Conditions: (i) HOAc, 135 °C; (ii) BBr_3, CH_2Cl_2, −78 °C to r.t.; (iii) Ag_2O, CH_2Cl_2, r.t.; (iv) $[Ir(\mu\text{-OMe})(cod)]_2$, 4,4′-di-*tert*-butyl-2,2′-bipyridyl, $B_2(pin)_2$, *tert*-butyl methyl ether/mesitylene, 70 °C; (v) mesityl bromide, SPhos Pd G2, methyltrioctylammonium chloride, toluene/K_2CO_3 aq., 100 °C; (vi) 1-bromo-3,5-di-*tert*-butylbenzene, SPhos Pd G2, methyltrioctylammonium chloride, toluene/K_2CO_3 aq., 100 °C; (vii) $CHCl_3$/HOAc, 75 °C for **FLAP1-H**, and 1,2-dichloroethane/HOAc, 95 °C for **FLAP1-OH** and **FLAP1-OH′**; (viii) butyl isocyanate, Et_3N, toluene, 110 °C. (b) Single crystal X-ray structure analysis of **FLAP1-OH′**. Thermal ellipsoids were drawn at the 50% probability level. Hydrogen atoms except for those in the OH groups and 3,5-di-*tert*-butylphenyl groups were omitted for clarity.

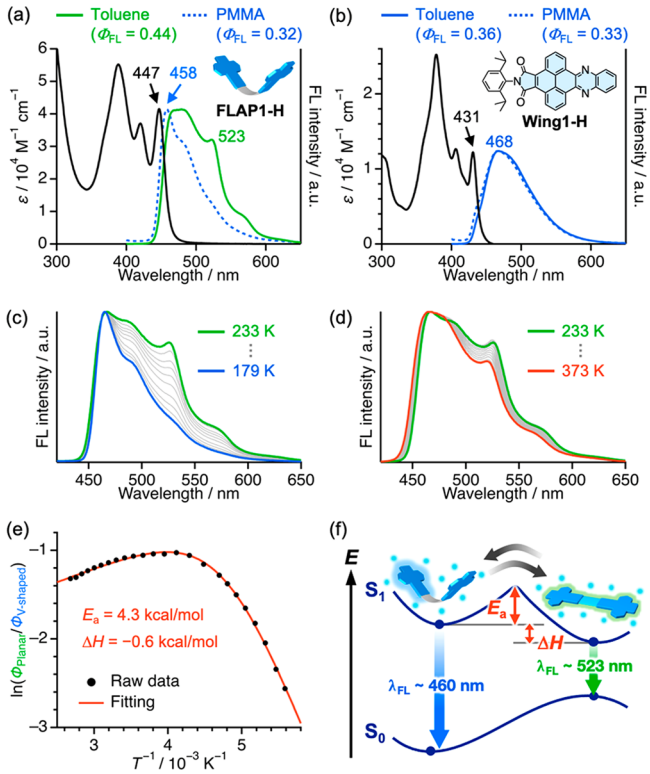

Figure 4. Optical properties of **FLAP1-H** in toluene. (a) Absorption and FL spectra of **FLAP1-H**, compared with (b) those of the reference compound (**Wing1-H**). (c,d) Variable-temperature FL spectra of **FLAP1-H**. (e) Stevens−Ban plot of the FL quantum yield ratio of the V-shaped and planar forms of **FLAP1-H** (see Section 4.2 in the SI for details on the spectral decomposition). (f) Energy profile that accounts for the dual FL of **FLAP1-H**.

equilibrium in the excited state (Figure 4f),[106,107] and the parameters related to this equilibrium (E_a and ΔH in S_1) were calculated by means of a Stevens−Ban plot[106,108] based on the area ratio of the two FL bands and the measurement temperature (SI, Section 4.2). The activation energy E_a was estimated to be 4.3 kcal/mol, and the enthalpy change ΔH was approximately −0.6 kcal/mol in S_1 (Figure 4e). The activation barrier of **FLAP1-H** for the S_1 planarization is much larger than the k_BT value at room temperature (0.6 kcal/mol at 298 K). This is in stark contrast to the results for **FLAP0-H**, which showed fast planarization dynamics in S_1.[93]

Computational Investigation of the Dual Fluorescence. Density functional theory (DFT) calculations were performed to gain insight into why the excited state planarization of **FLAP1-H** was suppressed in solution. Model compounds in which the 2,6-diisopropylphenyl groups of the original compounds were replaced by hydrogen atoms (denoted **FLAP0′**, **FLAP1′**, and **Wing1′**) were used for these computations. Although the calculation results were found to be sensitive to the level of theory, we adopted the PBE0/6-31+G(d)/PCM(toluene) level because the calculated absorption wavelengths of **Wing1′** were close to the experimental results, and the shape of the S_1 energy diagram of **FLAP1′** qualitatively agreed with the Stevens−Ban plot (SI, Section 5.3). Figures 5a and 5b show the calculated energy profiles of **FLAP0′** and **FLAP1′** in the S_0 and S_1 states as a function of the COT bending angle (increments of 2.5°). In S_0, the bent forms ($\theta \approx 40°$) were the most stable for both FLAPs due to the ring strain of COT, and conformational relaxation in S_1 occurs from these bent structures. Interestingly, the energy diagram of the S_1 state was quite different between **FLAP0′** and **FLAP1′**: **FLAP0′** partially flattened to a shallow V-shaped form (θ = 29.5°) followed by a complete planarization with a very small energy barrier (~0.2 kcal/mol), consistent with the observed green FL (inset in Figure 5a) and previously reported ultrafast dynamics in the excited state, whereas **FLAP1′** showed a larger energy barrier (~1.3 kcal/mol) between the bent and planar forms. Although these results were qualitative, the difference in the planarization behavior could be explained from the viewpoint of molecular orbital distribution in the bent S_1 geometries. In **FLAP0′**, the frontier orbitals were delocalized over the whole molecular frame, including the central COT ring (Figure 5c). Since the double bond character of the single bonds between the *cis*-olefins and the anthraceneimide units is enhanced in the S_1 electronic configuration, the conformational planarization is favorable in the excited state. On the other hand, the LUMO of **FLAP1′** was localized on the electron-withdrawing imide

https://doi.org/10.1021/jacs.1c12955
J. Am. Chem. Soc. 2022, 144, 2804−2815

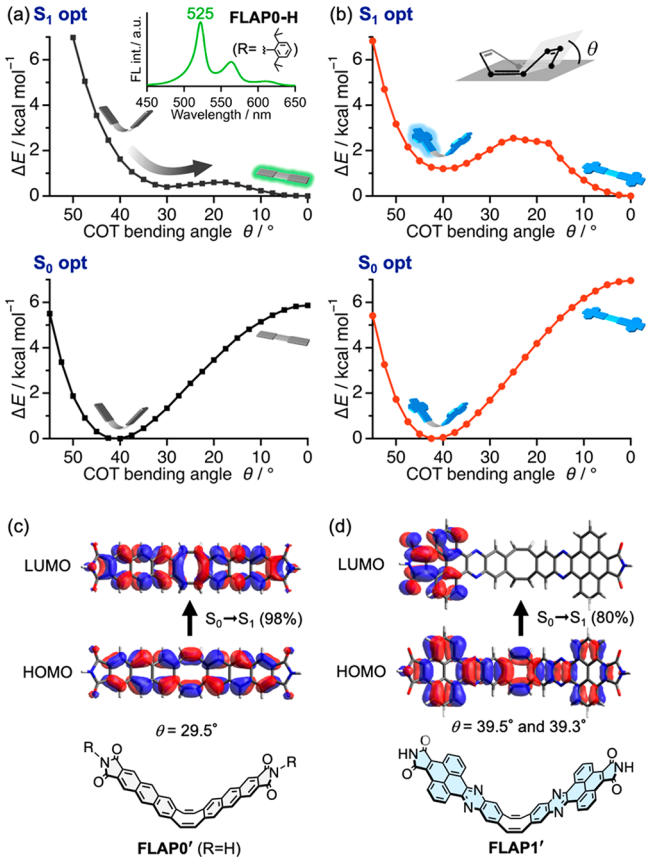

Figure 5. (a,b) S_1 (top) and S_0 (bottom) energy profiles of (a) **FLAP0′** and (b) **FLAP1′** obtained by (TD-)DFT calculations. The inset in (a) shows the FL spectrum of **FLAP0-H**. The COT bending angle θ was defined by the dihedral angle shown in the inset in (b). (c,d) Kohn−Sham orbitals of **FLAP0′** and **FLAP1′** displaying the distinct S_1 electronic character at the local minimum in S_1. Geometry optimizations were performed at the (TD-)PBE0/6-31+G(d)/PCM-(toluene) level.

moiety without contribution from the COT moiety (Figure 5d), suggesting that planarization in S_1 was less favorable. This difference in the orbital distribution is also consistent with the charge-transfer (CT) nature of the FL from the bent form of **FLAP1-H**, experimentally evaluated by a Lippert−Mataga plot (SI, Section 4.4).[109,110] It is worth noting that the FL derived from the planar form, peaked at 523 nm in toluene, showed less solvent dependence (Figure S4.13), consistent with the similarly delocalized HOMO and LUMO over the planar molecular frame (θ = 0°) of **FLAP1′** (Figure S5.14). The excited-state engineering based on the molecular orbital (de)localization is useful for designing dual-fluorescence molecules with the desired optical properties.

Improved Dynamic Range of the FL Spectral Response. Once the photophysical properties of **FLAP1-H** in solution were clarified, we next sought to investigate the FL response of **FLAP1-OH** as a force probe in a stretched polyurethane elastomer. Since the FL spectrum of **FLAP1-BC** (bearing the butylcarbamoyloxy groups at the termini) in toluene was similar to that of **FLAP1-H** (Figure S4.3), it was assumed that the mesityl groups and the urethane moieties would not substantially affect the photophysical properties when the force probe was introduced into polyurethane. First, **FLAP1-OH** was incorporated into segmented polyurethane (SPU) composed of poly(tetrahydrofuran) (PTHF), methylenediphenyl 4,4′-diisocyanate (MDI), and 1,4-butanediol (BDO). This is a widely used polymer into which various mechanophores have been introduced,[40] and 0.1−0.2 mm thick dumbbell-shaped specimens (**SPU1**) were prepared (Figure 6a). In the same way, the following three polymers were prepared for control experiments: (1) **SPU0**, which was chemically doped (covalently incorporated) with **FLAP0-OH**, (2) **SPU1-BC**, which was physically (noncovalently) doped with **FLAP1-BC**, and (3) **SPU2**, which was not doped with any force probe (Figure S6.1).

The synthesized polyurethanes were characterized by ^{1}H NMR spectroscopy (Figures S6.2−S6.5), and the ratio of soft segments to hard segments was confirmed to be 1:2.3, the same as the preparation ratio. In contrast, ^{1}H NMR signal of the incorporated force probe was not detectable due to the minimal amount of probe added. In addition, the thermal properties of the synthesized SPUs were measured by differential scanning calorimetry (DSC), and the results were comparable to those of similar polyurethanes that were previously reported (Figure S6.7).[78]

To investigate the force probe function of **FLAP1-OH**, we performed tensile tests of the prepared specimens and plotted engineering stress−strain curves (Figure 6b). The mechanical properties of the synthesized SPUs were comparable regardless of the presence of the probe, indicating that the addition of the flapping force probe had little effect on the mechanical properties. DSC analysis also indicated negligible influence of the probe on the thermal properties of the SPUs (Figure S6.7). The FL spectrum of **SPU1** was monitored during the tensile tests (Figure 6c). The relative intensity of the FL band at 472 nm, corresponding to the bent form of FLAP, decreased upon stretching, and that of the FL peak at 533 nm concomitantly increased with the appearance of a characteristic vibrational band at 575 nm, which was attributed to the planarized form of FLAP. The planarization of FLAP is also supported by the change in absorption spectra (Figure 6d, S6.15). When the 0.6 mm thick **SPU1** specimen was stretched, an absorption band appeared at longer wavelengths region (450−550 nm), indicating that FLAP was mechanically planarized in the ground state. The absorption tendency is more pronounced in a cross-linked polyurethane (Figure S7.8d). The distinct blue-to-green FL color change occurred rapidly and reversibly and could be clearly observed by the naked eye (Supporting Movie S1). The reversible FL spectral change was also confirmed using the tensile tester (Figure S6.10), although gradual photodegradation of the probe was observed in multiple loading−unloading cycles (Figure S6.11). Note that FRET-induced FL perturbation could be ignored because the average distance between the fluorescent probes was estimated to be approximately 20 nm (SI, Section 6.1), much longer than that permitting FRET (<10 nm).

The ratiometric FL analysis was performed by plotting the ratio of the FL intensity at 533 and 472 nm (I_{533}/I_{472}) against stress (Figure 6e). The FL intensity ratio increased monotonically from approximately 0.3 to ∼11 for **SPU1**. In contrast, when the same measurement was performed for **SPU0**, the FL intensity ratio reached only ∼2 (Figure S6.12). The wider dynamic range of the FL ratio of **FLAP1** is an important advantage of the new flapping force probe. Since **FLAP0** and **FLAP1** possess the same flexible hinge (COT), the distinct FL response should not be attributed to the difference in the percentage of stressed probes, but the difference in the FL quantum yields at the bent and planar forms. Indeed, the FL

https://doi.org/10.1021/jacs.1c12955
J. Am. Chem. Soc. 2022, 144, 2804−2815

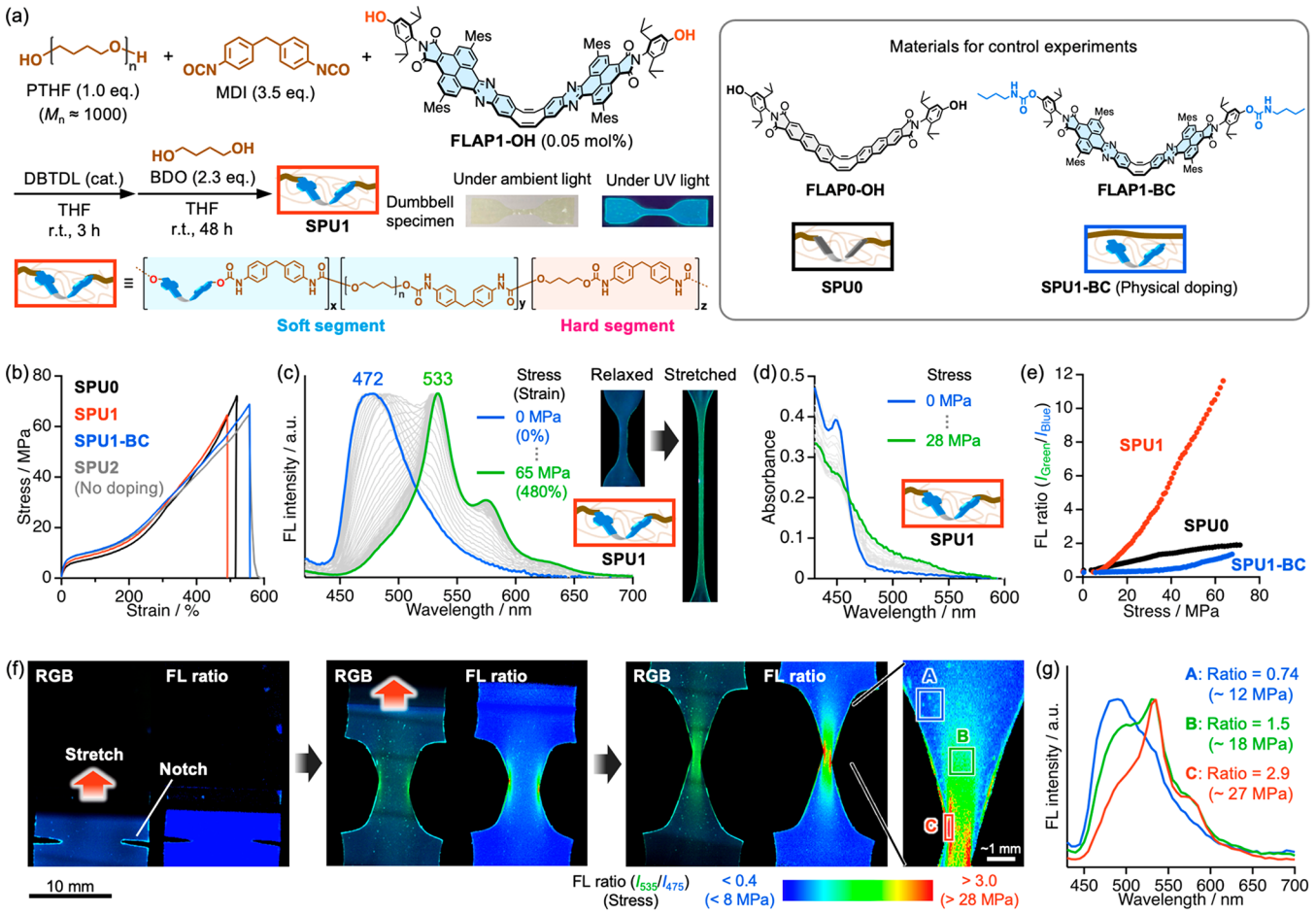

Figure 6. (a) Synthesis of a segmented polyurethane elastomer (**SPU1**) that is chemically doped with **FLAP1-OH** as a force probe. (b) Stress–strain curves of different SPUs. (c) FL spectral change of **SPU1** during the tensile test. Photographs of the specimen under UV light are shown on the right side. (d) Absorption spectral change of **SPU1** during the tensile test. (e) FL intensity ratio plotted against nominal stress in the tensile test. I_{533nm}/I_{472nm} was used as the ratio for **SPU1** and **SPU1-BC**, and I_{525nm}/I_{474nm} was used for **SPU0**. (f) Photographs (RGB) and stress mapping (FL ratio) of the notched **SPU1** film. The images were acquired using a hyperspectral camera, and the photographs were reconstructed from the RGB channels (R = 700 nm, G = 545 nm, B = 480 nm). (g) FL spectra averaged over the regions A–C shown in the left panel (bandwidth: 5 nm), and the estimated local stress based on the calibration in the panel (e). Strain rate: 0.17 s^{-1} for the panels (b–e), and 0.2 min^{-1} for the panel (f).

intensity of **SPU1** significantly increased upon stretching (Figure S6.13b), suggesting a large FL quantum yield of **FLAP1** in the planar form. The FL spectra of the negative control specimen **SPU1-BC** showed little response upon stretching, as expected. Only when the **SPU1-BC** film was strongly stretched over 40 MPa stress, a small spectral change was observed (Figure S6.9), which might be related to the strain-induced crystallization of the polymer chains (Figure S6.14) or the hydrogen bonding between urethane moieties of **FLAP1-BC** and polyurethane chains.

Ratiometric FL imaging of the notched **SPU1** specimen was performed with a hyperspectral camera (Figure 6f). As shown in Supporting Movie S2, the FL intensity ratio increased in the crack front region just before the crack propagation, while it returned to a small value in the corresponding region after the crack propagation was completed. From the relationship between the stress and the FL ratio in Figure 6e, the average stress was estimated in each of the three regions A–C (Figure 6f and 6g). As a result, the local stress distribution in the range of 12–27 MPa was visualized with submillimeter spatial resolution. Thus, the flapping force probe with wider dynamic range would be useful for mapping local stress distribution more clearly.

Synthesis of Cross-Linked Polyurethanes and the Preparation of the Organogels. To investigate the efficacy of the force probe **FLAP1** in wet materials, cross-linked polyurethanes (PUs) were synthesized (Figure 7a). Poly(tetrahydrofuran) (PTHF) and hexamethylene diisocyanate (HDI) were selected as the main chain components, while triethanolamine (TEA) was used as the cross-linker.[91] The cross-linking density, defined as the molar fraction of TEA to all monomers, was set to 8.7%. A trace amount of **FLAP1-OH** (0.01 mol % to HDI) was added to the mixed monomer solution, and polymerization was initiated by a tin catalyst (DBTDL). The resulting solution was poured into a poly(tetrafluoroethylene) (PTFE) mold to prepare a dry cylindrical specimen of **PU1**. The negligible influence of the probes on thermal and mechanical properties of the dry PUs were again confirmed (Figures S7.4 and S7.5). Organogels were prepared by swelling the cross-linked polyurethane **PU1** with organic solvents. We selected cyclopentyl methyl ether (CPME) as the solvent because the short and long λ_{FL} bands of **FLAP1-H** are well separated in CPME and thus suitable for the reliable spectral decomposition (Figure S4.11b). In addition, since CPME has a high boiling point (106 °C), contribution of the solvent evaporation is negligible during

https://doi.org/10.1021/jacs.1c12955
J. Am. Chem. Soc. 2022, 144, 2804–2815

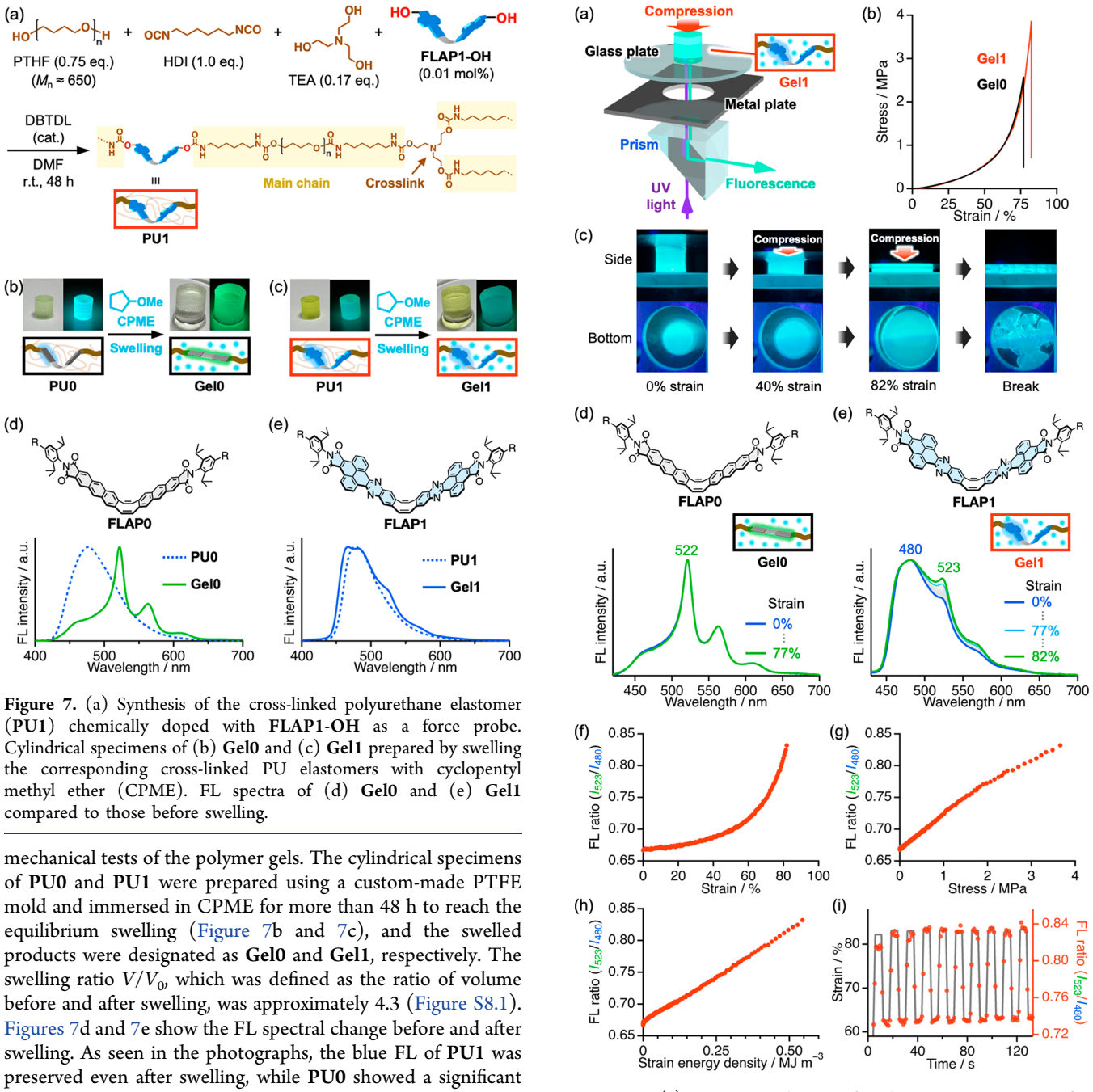

Figure 7. (a) Synthesis of the cross-linked polyurethane elastomer (**PU1**) chemically doped with **FLAP1-OH** as a force probe. Cylindrical specimens of (b) **Gel0** and (c) **Gel1** prepared by swelling the corresponding cross-linked PU elastomers with cyclopentyl methyl ether (CPME). FL spectra of (d) **Gel0** and (e) **Gel1** compared to those before swelling.

mechanical tests of the polymer gels. The cylindrical specimens of **PU0** and **PU1** were prepared using a custom-made PTFE mold and immersed in CPME for more than 48 h to reach the equilibrium swelling (Figure 7b and 7c), and the swelled products were designated as **Gel0** and **Gel1**, respectively. The swelling ratio V/V_0, which was defined as the ratio of volume before and after swelling, was approximately 4.3 (Figure S8.1). Figures 7d and 7e show the FL spectral change before and after swelling. As seen in the photographs, the blue FL of **PU1** was preserved even after swelling, while **PU0** showed a significant FL change when swelled. Thus, **FLAP0** in **Gel0** underwent the spontaneous S_1 planarization when surrounded by solvent molecules, while the S_1 planarization of **FLAP1** in **Gel1** was almost completely suppressed due to the above-mentioned excited-state engineering. Here, the observed planarization of **FLAP0** in **Gel0** was not attributed to swelling pressure, unlike the activation of mechanophores by swelling of glassy PMMA,[111,112] because the percentages of the stressed probes **FLAP0** and **FLAP1** are expected to be almost comparable when doped in the same host polymer. Indeed, the percentages of the stressed probes in a stretched PU elastomer were experimentally estimated to be up to 30−40% for both probes, using an internal standard of a red emitter, Rhodamine 640 (SI, Section 7.5).

Fluorescence Response upon Compressing the Organogels. Compression tests of the cylindrical gel specimens with the experimental setup shown in Figure 8a

Figure 8. (a) Experimental setup for the compression test of a cylindrical specimen of **Gel1**. (b) Nominal stress−strain curves of the gels. (c) Photographs of the compression process of **Gel1** under UV light (365 nm). (d,e) FL spectral change of (d) **Gel0** and (e) **Gel1** during the compression test. (f−h) FL intensity ratio plotted against (f) strain, (g) stress, and (h) strain energy density in the compression test. (i) Reversible response of the FL ratio for ten cycles of compression and release. Strain rate: ∼0.27 min^{-1} for the panels (b−h), and 0.14 s^{-1} for the panel (i).

were successfully conducted (Supporting Movie S3). We note that the tensile tests using the dumbbell specimens were difficult due to the fragility of the gel materials. Although the fracture strain was considerably dependent on the individual samples, **Gel0** and **Gel1** showed the similar stress−strain curves, as shown in Figure 8b. In contrast, the FL spectra of **Gel0** and **Gel1** showed distinct behaviors upon the compression, where the bottom surface of the cylindrical

https://doi.org/10.1021/jacs.1c12955
J. Am. Chem. Soc. 2022, 144, 2804−2815

specimen was observed (Figure 8c). While **Gel0** showed negligible FL change upon compression (Figure 8d), a FL band at 523 nm emitted from the planar form of **FLAP1** became more pronounced for **Gel1** (Figure 8e). The ratio of the FL intensity at 480 and 523 nm was monitored during the compression test, whose values were plotted against the nominal (engineering) strain, stress, and strain energy density in Figures 8f, 8g, and 8h, respectively. While the dynamic range of the FL response of **Gel1** was limited due to the fragility of this material compared to that of the solvent-free **PU1**, quantitative analysis was effectively performed with a sufficient signal-to-noise ratio. On the other hand, the control material, **Gel0**, yielded negative results in the spectroscopic analysis (Figure S9.3). Interestingly, the FL ratio at the center of compressed **Gel1** was slightly higher than the periphery (Supporting Movie S4). The values of nominal stress and FL intensity ratio in Figure 8 were obtained as spatially averaged ones.

Importantly, the FL response of **Gel1** started from the earlier stage, compared with the corresponding solvent-free elastomer. In the low-stress region (<1 MPa), **Gel1** showed a remarkable FL response (Figures 8g), while **PU1** did not show a change in the FL ratio (Figures S7.8c). **Gel1** showed an excellent linear relationship between the FL ratio and the strain energy density, defined as the area under the stress−strain curve (Figure 8h, S9.5). These results suggested that the polymer chains were prestretched by swelling before compression, although the degree of stretching was not remarkable. The FL response of **Gel1** was reversible, and a cycling test with a higher strain rate showed that the FL ratio could quickly respond to the strain or stress (Figure 8i and S9.6).

Real-Time Stress Mapping of the Compressed Organogels by Ratiometric Fluorescence Imaging. To demonstrate the force probe function of **FLAP1** under a nonuniform stress distribution in gels, we applied pressure to the plate-shaped **Gel1** with metal stamps using the experimental setup shown in Figure 9a−b. With the naked eye, it was difficult to distinguish the degree of the mechanical stress applied by each alphabetical stamp. However, ratiometric FL imaging showed that the more local stress was applied by the "L" and "P" metal stamps than by the "F" and "A" stamps (Figure 9c and Supporting Movie S5), which probably originated from the slightly different thicknesses of these metal stamps. Since the bottom area of the cylindrical specimen in Figure 8 largely changed upon compression, a calibration curve was plotted to estimate the true stress from the observed FL intensity ratio, by tracking and correcting the change in the bottom area (Figure 9d and S9.7). According to this estimation, true compression stresses applied in the regions A−C of **Gel1** were quantitatively evaluated to lie in the range of 0−1 MPa with a submillimeter spatial resolution (Figure 9c and 9e).

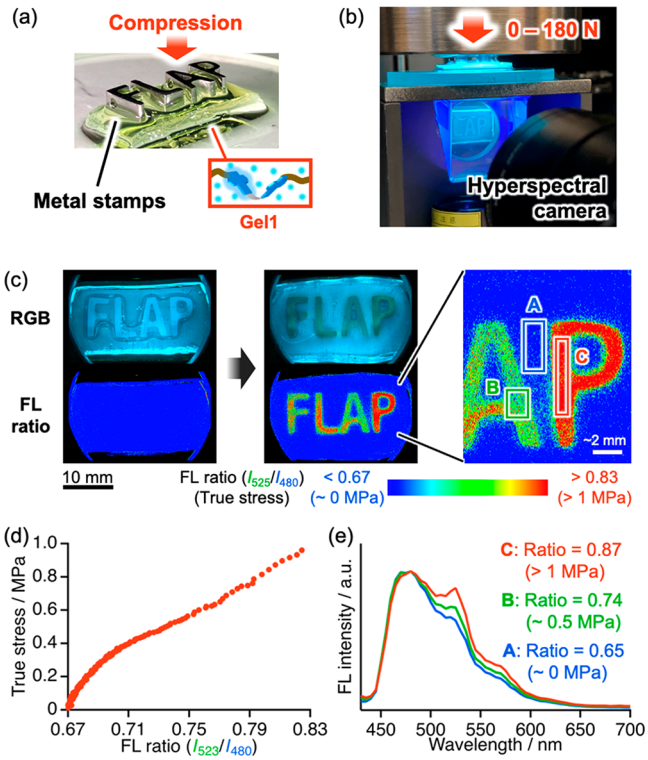

Figure 9. (a) Photograph of the metal stamps placed on **Gel1** to apply a nonuniform stress distribution. (b) Photograph of the setup for observing the bottom of the gel with a hyper spectral camera through a prism. (c) Photographs (RGB) and stress mapping (FL ratio) of **Gel1** compressed by the metal stamps. The images were obtained by following the protocol described in Figure 6. (d) Calibration curve for estimating the true stress from the observed FL ratio of **Gel1**, which was obtained from Figure 8g with the consideration of the change in the bottom area of the gels. (e) FL spectra averaged over the regions A−C shown in the panel (c) (bandwidth: 5 nm), and the local true stress estimated from the calibration curve in the panel (d).

CONCLUSIONS

A ratiometric flapping force probe (FLAP) that can be used to evaluate the nanoscale stress concentration transmitted in a polymer chain network of organogels was developed. A previously reported FLAP bearing anthraceneimide wings showed only a negligible fluorescence response to the mechanical stress under solvated conditions because undesirable planarization spontaneously occurred in the excited state even without stress. In this study, we raised the excited-state energy barrier by changing the flapping wings into the pyreneimide units, which suppressed the spontaneous excited-state planarization and allowed this molecule to serve as a force probe even in wet environments. The modified force probe also had a wider dynamic range of the stress-induced fluorescence spectral change in solvent-free elastomers. Ratiometric fluorescence imaging of the molecular-level stress concentration was demonstrated in a real-time and reversible manner both for the stretched elastomers and compressed gels. FLAPs are expected to be useful for studying the polymer chain dynamics of structurally designed tough materials.[8,9] Although the mechanochemistry of hydrogels has been discussed in several studies,[58,89,90,113,114] increasing the hydrophilicity of the FLAP probe would lead to new molecular technology, such as membrane tension probes that work in cells.[96,115−117]

ASSOCIATED CONTENT

Supporting Information

The Supporting Information is available free of charge at https://pubs.acs.org/doi/10.1021/jacs.1c12955.

Experimental and theoretical details (PDF)
Movie S1 showing the reversible FL response of the **SPU1** film (MP4)

https://doi.org/10.1021/jacs.1c12955
J. Am. Chem. Soc. 2022, 144, 2804−2815

Movie S2 showing the ratiometric imaging of the stress applied to the notched **SPU1** film (MP4)

Movie S3 showing compression of the cylindrical **Gel1** specimen (MP4)

Movie S4 showing the distribution of the FL ratio of the cylindrical **Gel1** specimen under compression (MP4)

Movie S5 showing the ratiometric imaging of the stress applied to **Gel1** by the metal stamps (MP4)

Accession Codes

CCDC 2122594−2122595 contain the supplementary crystallographic data for this paper. These data can be obtained free of charge via www.ccdc.cam.ac.uk/data_request/cif, or by emailing data_request@ccdc.cam.ac.uk, or by contacting The Cambridge Crystallographic Data Centre, 12 Union Road, Cambridge CB2 1EZ, UK; fax: +44 1223 336033.

AUTHOR INFORMATION

Corresponding Author

Shohei Saito − *Graduate School of Science, Kyoto University, Kyoto 606-8502, Japan;* orcid.org/0000-0003-1863-9956; Email: saito.shohei.4c@kyoto-u.ac.jp

Author

Takuya Yamakado − *Graduate School of Science, Kyoto University, Kyoto 606-8502, Japan;* orcid.org/0000-0002-0730-2904

Complete contact information is available at: https://pubs.acs.org/10.1021/jacs.1c12955

Notes

The authors declare no competing financial interest.

ACKNOWLEDGMENTS

JST PRESTO (FRONTIER) and JST FOREST Grant Numbers JPMJPR16P6 (S.S.) and JPMJFR201L (S.S.), JSPS KAKENHI Grant Number JP21H01917 (S.S), JP21H05482 (S.S), and JSPS Fellowships Grant Number JP19J22034 (T.Y). Inoue Foundation for Science (S.S.) and Toray Science Foundation (S.S.). We thank Prof. Hideki Yorimitsu and Prof. Hiroshi Kamitakahara (Kyoto University) for their help with the high-resolution mass spectrometry measurements.

REFERENCES

(1) Li, J.; Mooney, D. J. Designing hydrogels for controlled drug delivery. *Nat. Rev. Mater.* **2016**, *1*, 16071.
(2) Lee, K. Y.; Mooney, D. J. Hydrogels for Tissue Engineering. *Chem. Rev.* **2001**, *101*, 1869−1880.
(3) Lim, H.-R.; Kim, H. S.; Qazi, R.; Kwon, Y.-T.; Jeong, J.-W.; Yeo, W.-H. Advanced Soft Materials, Sensor Integrations, and Applications of Wearable Flexible Hybrid Electronics in Healthcare, Energy, and Environment. *Adv. Mater.* **2020**, *32*, 1901924.
(4) Hines, L.; Petersen, K.; Lum, G. Z.; Sitti, M. Soft Actuators for Small-Scale Robotics. *Adv. Mater.* **2017**, *29*, 1603483.
(5) Yang, C.; Suo, Z. Hydrogel ionotronics. *Nat. Rev. Mater.* **2018**, *3*, 125−142.
(6) Dong, Y.; Ramey-Ward, A. N.; Salaita, K. Programmable Mechanically Active Hydrogel-Based Materials. *Adv. Mater.* **2021**, *33*, 2006600.
(7) Calvert, P. Hydrogels for Soft Machines. *Adv. Mater.* **2009**, *21*, 743−756.
(8) Creton, C. 50th Anniversary Perspective: Networks and Gels: Soft but Dynamic and Tough. *Macromolecules* **2017**, *50*, 8297−8316.
(9) Zhao, X.; Chen, X.; Yuk, H.; Lin, S.; Liu, X.; Parada, G. Soft Materials by Design: Unconventional Polymer Networks Give Extreme Properties. *Chem. Rev.* **2021**, *121*, 4309−4372.
(10) Gong, J. P.; Katsuyama, Y.; Kurokawa, T.; Osada, Y. Double-Network Hydrogels with Extremely High Mechanical Strength. *Adv. Mater.* **2003**, *15*, 1155−1158.
(11) Gong, J. P. Why are double network hydrogels so tough? *Soft Matter* **2010**, *6*, 2583−2590.
(12) Matsuda, T.; Kawakami, R.; Namba, R.; Nakajima, T.; Gong, J. P. Mechanoresponsive self-growing hydrogels inspired by muscle training. *Science* **2019**, *363*, 504−508.
(13) Wang, Z.; Zheng, X.; Ouchi, T.; Kouznetsova, T. B.; Beech, H. K.; Av-Ron, S.; Matsuda, T.; Bowser, B. H.; Wang, S.; Johnson, J. A.; Kalow, J. A.; Olsen, B. D.; Gong, J. P.; Rubinstein, M.; Craig, S. L. Toughening hydrogels through force-triggered chemical reactions that lengthen polymer strands. *Science* **2021**, *374*, 193−196.
(14) Tuncaboylu, D. C.; Sari, M.; Oppermann, W.; Okay, O. Tough and Self-Healing Hydrogels Formed via Hydrophobic Interactions. *Macromolecules* **2011**, *44*, 4997.
(15) Sun, J.-Y.; Zhao, X.; Illeperuma, W. R. K.; Chaudhuri, O.; Oh, K. H.; Mooney, D. J.; Vlassak, J. J.; Suo, Z. Highly stretchable and tough hydrogels. *Nature* **2012**, *489*, 133−136.
(16) Guo, M.; Pitet, L. M.; Wyss, H. M.; Vos, M.; Dankers, P. Y. W.; Meijer, E. W. Tough Stimuli-Responsive Supramolecular Hydrogels with Hydrogen-Bonding Network Junctions. *J. Am. Chem. Soc.* **2014**, *136*, 6969−6977.
(17) Dai, X.; Zhang, Y.; Gao, L.; Bai, T.; Wang, W.; Cui, Y.; Liu, W. A Mechanically Strong, Highly Stable, Thermoplastic, and Self-Healable Supramolecular Polymer Hydrogel. *Adv. Mater.* **2015**, *27*, 3566.
(18) Lei, H.; Dong, L.; Li, Y.; Zhang, J.; Chen, H.; Wu, J.; Zhang, Y.; Fan, Q.; Xue, B.; Qin, M.; Chen, B.; Cao, Y.; Wang, W. Stretchable hydrogels with low hysteresis and antifatigue fracture based on polyprotein cross-linkers. *Nat. Commun.* **2020**, *11*, 4032.
(19) Haraguchi, K.; Takehisa, T. Nanocomposite Hydrogels: A Unique Organic−Inorganic Network Structure with Extraordinary Mechanical, Optical, and Swelling/De-swelling Properties. *Adv. Mater.* **2002**, *14*, 1120−1124.
(20) Gao, G.; Du, G.; Sun, Y.; Fu, J. Self-Healable, Tough, and Ultrastretchable Nanocomposite Hydrogels Based on Reversible Polyacrylamide/Montmorillonite Adsorption. *ACS Appl. Mater. Interfaces* **2015**, *7*, 5029−5037.
(21) Shao, C.; Chang, H.; Wang, M.; Xu, F.; Yang, J. High-Strength, Tough, and Self-Healing Nanocomposite Physical Hydrogels Based on the Synergistic Effects of Dynamic Hydrogen Bond and Dual Coordination Bonds. *ACS Appl. Mater. Interfaces* **2017**, *9*, 28305−28318.
(22) Li, H.-J.; Jiang, H.; Haraguchi, K. Ultrastiff, Thermoresponsive Nanocomposite Hydrogels Composed of Ternary Polymer−Clay−Silica Networks. *Macromolecules* **2018**, *51*, 529−539.
(23) Lin, S.; Lui, X.; Liu, J.; Yuk, H.; Loh, H.-C.; Parada, G. A.; Settens, C.; Song, J.; Masic, A.; McKinley, G. H.; Zhao, X. Anti-fatigue-fracture hydrogels. *Sci. Adv.* **2019**, *5*, eaau8528.
(24) Liu, C.; Morimoto, N.; Jiang, L.; Kawahara, S.; Noritomi, T.; Yokoyama, H.; Mayumi, K.; Ito, K. Tough hydrogels with rapid self-reinforcement. *Science* **2021**, *372*, 1078−1081.
(25) Zhao, X. Multi-scale multi-mechanism design of tough hydrogels: building dissipation into stretchy networks. *Soft Matter* **2014**, *10*, 672−687.
(26) Ducrot, E.; Chen, Y.; Bulters, M.; Sijbesma, R. P.; Creton, C. Toughening Elastomers with Sacrificial Bonds and Watching Them Break. *Science* **2014**, *344*, 186−189.
(27) Neal, J. A.; Mozhdehi, D.; Guan, Z. Enhancing Mechanical Performance of a Covalent Self-Healing Material by Sacrificial Noncovalent Bonds. *J. Am. Chem. Soc.* **2015**, *137*, 4846−4850.
(28) Filippidi, E.; Cristiani, T. R.; Eisenbach, C. D.; Waite, J. H.; Israelachvili, J. N.; Ahn, B. K.; Valentine, M. T. Toughening elastomers using mussel-inspired iron-catechol complexes. *Science* **2017**, *358*, 502−505.

(29) Wu, J.; Cai, L.-H.; Weitz, D. A. Tough Self-Healing Elastomers by Molecular Enforced Integration of Covalent and Reversible Networks. *Adv. Mater.* **2017**, *29*, 1702616.
(30) Gotoh, H.; Liu, C.; Imran, A. B.; Hara, M.; Seki, T.; Mayumi, K.; Ito, K.; Takeoka, Y. Optically transparent, high-toughness elastomer using a polyrotaxane cross-linker as a molecular pulley. *Sci. Adv.* **2018**, *4*, eaat7629.
(31) Sakai, H.; Aoki, D.; Seshimo, K.; Mayumi, K.; Nishitsuji, S.; Kurose, T.; Ito, H.; Otsuka, H. Visualization and Quantitative Evaluation of Toughening Polymer Networks by a Sacrificial Dynamic Cross-Linker with Mechanochromic Properties. *ACS Macro Lett.* **2020**, *9*, 1108−1113.
(32) Sakai, T.; Matsunaga, T.; Yamamoto, Y.; Ito, C.; Yoshida, R.; Suzuki, S.; Sasaki, N.; Shibayama, M.; Chung, U. Design and Fabrication of a High-Strength Hydrogel with Ideally Homogeneous Network Structure from Tetrahedron-like Macromonomers. *Macromolecules* **2008**, *41*, 5379−5384.
(33) Sakai, T.; Akagi, Y.; Matsunaga, T.; Kurakazu, M.; Chung, U.; Shibayama, M. Highly Elastic and Deformable Hydrogel Formed from Tetra-arm Polymers. *Macromol. Rapid Commun.* **2010**, *31*, 1954−1959.
(34) Kamata, H.; Akagi, Y.; Kayasuga-Kariya, Y.; Chung, U.; Sakai, T. Nonswellable" Hydrogel Without Mechanical Hysteresis. *Science* **2014**, *343*, 873−875.
(35) Li, X.; Nakagawa, S.; Tsuji, Y.; Watanabe, N.; Shibayama, M. Polymer gel with a flexible and highly ordered three-dimensional network synthesized via bond percolation. *Sci. Adv.* **2019**, *5*, eaax8647.
(36) Okumura, Y.; Ito, K. The Polyrotaxane Gel: A Topological Gel by Figure-of-Eight Cross-links. *Adv. Mater.* **2001**, *13*, 485−487.
(37) Imran, A. B.; Esaki, K.; Gotoh, H.; Seki, T.; Ito, K.; Sakai, Y.; Takeoka, Y. Extremely stretchable thermosensitive hydrogels by introducing slide-ring polyrotaxane cross-linkers and ionic groups into the polymer network. *Nat. Commun.* **2014**, *5*, 4124.
(38) Choi, S.; Kwon, T.; Coskun, A.; Choi, J. W. Highly elastic binders integratingpolyrotaxanes for siliconmicroparticle anodes in lithiumion batteries. *Science* **2017**, *357*, 279−283.
(39) Chen, Y.; Sanoja, G.; Creton, C. Mechanochemistry unveils stress transfer during sacrificial bond fracture of tough multiple network elastomers. *Chem. Sci.* **2021**, *12*, 11098−11108.
(40) Chen, Y.; Mellot, G.; van Luijk, D.; Creton, C.; Sijbesma, R. P. Mechanochemical tools for polymer materials. *Chem. Soc. Rev.* **2021**, *50*, 4100−4140.
(41) O'Neill, R. T.; Boulatov, R. The many flavours of mechanochemistry and its plausible conceptual underpinnings. *Nat. Rev. Chem.* **2021**, *5*, 148−167.
(42) Davis, D. A.; Hamilton, A.; Yang, J.; Cremar, L. D.; Van Gough, D.; Potisek, S. L.; Ong, M. T.; Braun, P. V.; Martinez, T. J.; White, S. R.; Moore, J. S.; Sottos, N. R. Force-Induced Activation of Covalent Bonds in Mechanoresponsive Polymeric Materials. *Nature* **2009**, *459*, 68−72.
(43) Gossweiler, G. R.; Kouznetsova, T. B.; Craig, S. L. Force-Rate Characterization of Two Spiropyran-Based Molecular Force Probes. *J. Am. Chem. Soc.* **2015**, *137*, 6148−6151.
(44) Lin, Y.; Barbee, M. H.; Chang, C.-C.; Craig, S. L. Regiochemical Effects on Mechanophore Activation in Bulk Materials. *J. Am. Chem. Soc.* **2018**, *140*, 15969−15975.
(45) Barbee, M. H.; Kouznetsova, T.; Barrett, S. L.; Gossweiler, G. R.; Lin, Y.; Rastogi, S. K.; Brittain, W. J.; Craig, S. L. Substituent Effects and Mechanism in a Mechanochemical Reaction. *J. Am. Chem. Soc.* **2018**, *140*, 12746−12750.
(46) Robb, M. J.; Kim, T. A.; Halmes, A. J.; White, S. R.; Sottos, N. R.; Moore, J. S. Regioisomer-Specific Mechanochromism of Naphthopyran in Polymeric Materials. *J. Am. Chem. Soc.* **2016**, *138*, 12328−12331.
(47) McFadden, M. E.; Robb, M. J. Force-Dependent Multicolor Mechanochromism from a Single Mechanophore. *J. Am. Chem. Soc.* **2019**, *141*, 11388−11392.
(48) Versaw, B. A.; McFadden, M. E.; Husic, C. C.; Robb, M. J. Designing Naphthopyran Mechanophores with Tunable Mechanochromic Behavior. *Chem. Sci.* **2020**, *11*, 4525−4530.
(49) Imato, K.; Otsuka, H. Reorganizable and stimuli-responsive polymers based on dynamic carbonecarbon linkages in diarylbibenzofuranones. *Polymer* **2018**, *137*, 395−413.
(50) Imato, K.; Irie, A.; Kosuge, T.; Ohishi, T.; Nishihara, M.; Takahara, A.; Otsuka, H. Mechanophores with a Reversible Radical System and Freezing-Induced Mechanochemistry in Polymer Solutions and Gels. *Angew. Chem., Int. Ed.* **2015**, *54*, 6168−6172.
(51) Imato, K.; Kanehara, T.; Ohishi, T.; Nishihara, M.; Yajima, H.; Ito, M.; Takahara, A.; Otsuka, H. Mechanochromic Dynamic Covalent Elastomers: Quantitative Stress Evaluation and Autonomous Recovery. *ACS Macro Lett.* **2015**, *4*, 1307−1311.
(52) Ishizuki, K.; Aoki, D.; Goseki, R.; Otsuka, H. Multicolor Mechanochromic Polymer Blends That Can Discriminate between Stretching and Grinding. *ACS Macro Lett.* **2018**, *7*, 556−560.
(53) Kosuge, T.; Zhu, X.; Lau, V. M.; Aoki, D.; Martinez, T. J.; Moore, J. S.; Otsuka, H. Multicolor Mechanochromism of a Polymer/Silica Composite with Dual Distinct Mechanophores. *J. Am. Chem. Soc.* **2019**, *141*, 1898−1902.
(54) Chen, Y.; Spiering, A. J. H.; Karthikeyan, S.; Peters, G. W. M.; Meijer, E. W.; Sijbesma, R. P. Mechanically Induced Chemiluminescence from Polymers Incorporating a 1,2-Dioxetane Unit in the Main Chain. *Nat. Chem.* **2012**, *4*, 559−562.
(55) Song, Y.-K.; Lee, K.-H.; Hong, W.-S.; Cho, S.-Y.; Yu, H.-C.; Chung, C.-M. Fluorescence sensing of microcracks based on cycloreversion of a dimeric anthracene moiety. *J. Mater. Chem.* **2012**, *22*, 1380−1386.
(56) Kabb, C. P.; O'Bryan, C. S.; Morley, C. D.; Angelini, T. E.; Sumerlin, B. S. Anthracene-based mechanophores for compression-activated fluorescence in polymeric networks. *Chem. Sci.* **2019**, *10*, 7702−7708.
(57) Göstl, R.; Sijbesma, R. P. π-extended anthracenes as sensitive probes for mechanical stress. *Chem. Sci.* **2016**, *7*, 370.
(58) Stratigaki, M.; Baumann, C.; van Breemen, L. C. A.; Heuts, J. P. A.; Sijbesma, R. P.; Göstl, R. Fractography of poly(*N*-isopropylacrylamide) hydrogel networks crosslinked with mechanofluorophores using confocal laser scanning microscopy. *Polym. Chem.* **2020**, *11*, 358−366.
(59) Baumann, C.; Stratigaki, M.; Centeno, S. P.; Göstl, R. Multicolor Mechanofluorophores for the Quantitative Detection of Covalent Bond Scission in Polymers. *Angew. Chem., Int. Ed.* **2021**, *60*, 13287−13293.
(60) Kato, S.; Ishizuki, K.; Aoki, D.; Goseki, R.; Otsuka, H. Freezing Induced Mechanoluminescence of Polymer Gels. *ACS Macro Lett.* **2018**, *7*, 1087−1091.
(61) Kato, S.; Furukawa, S.; Aoki, D.; Goseki, R.; Oikawa, K.; Tsuchiya, K.; Shimada, N.; Maruyama, A.; Numata, K.; Otsuka, H. Crystallization-Induced Mechanofluorescence for Visualization of Polymer Crystallization. *Nat. Commun.* **2021**, *12*, 126.
(62) Brown, C. L.; Craig, S. L. Molecular engineering of mechanophore activity for stress-responsive polymeric materials. *Chem. Sci.* **2015**, *6*, 2158−2165.
(63) Li, J.; Nagamani, C.; Moore, J. S. Polymer Mechanochemistry: From Destructive to Productive. *Acc. Chem. Res.* **2015**, *48*, 2181−2190.
(64) Deneke, N.; Rencheck, M. L.; Davis, C. S. An engineer's introduction to mechanophores. *Soft Matter* **2020**, *16*, 6230−6252.
(65) Chen, Z.; Mercer, J. A. M.; Zhu, X.; Romaniuk, J. A. H.; Pfattner, R.; Cegelski, L.; Martinez, T. J.; Burns, N. Z.; Xia, Y. Mechanochemical unzipping of insulating polyladderene to semiconducting polyacetylene. *Science* **2017**, *357*, 475−479.
(66) Stratigaki, M.; Göstl, R. Methods for Exerting and Sensing Force in Polymer Materials Using Mechanophores. *ChemPlusChem.* **2020**, *85*, 1095−1103.
(67) He, S.; Stratigaki, M.; Centeno, S. P.; Dreuw, A.; Göstl, R. Tailoring the Properties of Optical Force Probes for Polymer Mechanochemistry. *Chem. Eur. J.* **2021**, *27*, 15889−15897.

(68) Chen, Y.; Yeh, C. J.; Qi, Y.; Long, R.; Creton, C. From force-responsive molecules to quantifying and mapping stresses in soft materials. *Sci. Adv.* **2020**, *6*, eaaz5093.
(69) Slootman, J.; Waltz, V.; Yeh, C. J.; Baumann, C.; Göstl, R.; Comtet, J.; Creton, C. Quantifying Rate- and Temperature-Dependent Molecular Damage in Elastomer Fracture. *Phys. Rev. X* **2020**, *10*, 041045.
(70) Chen, Y.; Sanoja, G.; Creton, C. Mechanochemistry unveils stress transfer during sacrificial bond fracture of tough multiple network elastomers. *Chem. Sci.* **2021**, *12*, 11098−11108.
(71) Chen, Y.; Yeh, C. J.; Guo, Q.; Qi, Y.; Long, R.; Creton, C. Fast reversible isomerization of merocyanine as a tool to quantify stress history in elastomers. *Chem. Sci.* **2021**, *12*, 1693−1701.
(72) Gossweiler, G. R.; Hewage, G. B.; Soriano, G.; Wang, Q.; Welshofer, G. W.; Zhao, X.; Craig, S. L. Mechanochemical Activation of Covalent Bonds in Polymers with Full and Repeatable Macroscopic Shape Recovery. *ACS Macro Lett.* **2014**, *3*, 216−219.
(73) Wang, T.; Zhang, N.; Dai, J.; Li, Z.; Bai, W.; Bai, R. Novel Reversible Mechanochromic Elastomer with High Sensitivity: Bond Scission and Bending-Induced Multicolor Switching. *ACS Appl. Mater. Interfaces* **2017**, *9*, 11874−11881.
(74) Filonenko, G. A.; Khusnutdinova, J. R. Dynamic Phosphorescent Probe for Facile and Reversible Stress Sensing. *Adv. Mater.* **2017**, *29*, 1700563.
(75) Filonenko, G. A.; Lugger, J. A. M.; Liu, C.; van Heeswijk, E. P. A.; Hendrix, M. M. R. M.; Weber, M.; Müller, C.; Hensen, E. J. M.; Sijbesma, R. P.; Pidko, E. A. Tracking Local Mechanical Impact in Heterogeneous Polymers with Direct Optical Imaging. *Angew. Chem., Int. Ed.* **2018**, *57*, 16385−16390.
(76) Qian, H.; Purwanto, N. S.; Ivanoff, D. G.; Halmes, A. J.; Sottos, N. R.; Moore, J. S. Fast, reversible mechanochromism of regioisomeric oxazine mechanophores: Developing in situ responsive force probes for polymeric materials. *Chem* **2021**, *7*, 1080−1091.
(77) Raisch, M.; Maftuhin, W.; Walter, M.; Sommer, M. A mechanochromic donor-acceptor torsional spring. *Nat. Commun.* **2021**, *12*, 4243.
(78) Sagara, Y.; Karman, M.; Verde-Sesto, E.; Matsuo, K.; Kim, Y.; Tamaoki, N.; Weder, C. Rotaxanes as Mechanochromic Fluorescent Force Transducers in Polymers. *J. Am. Chem. Soc.* **2018**, *140*, 1584−1587.
(79) Sagara, Y.; Karman, M.; Seki, A.; Pannipara, M.; Tamaoki, N.; Weder, C. Rotaxane-Based Mechanophores Enable Polymers with Mechanically Switchable White Photoluminescence. *ACS Cent. Sci.* **2019**, *5*, 874−881.
(80) Muramatsu, T.; Sagara, Y.; Traeger, H.; Tamaoki, N.; Weder, C. Mechanoresponsive Behavior of a Polymer-Embedded Red-Light Emitting Rotaxane Mechanophore. *ACS Appl. Mater. Interfaces* **2019**, *11*, 24571−24576.
(81) Muramatsu, T.; Okado, Y.; Traeger, H.; Schrettl, S.; Tamaoki, N.; Weder, C.; Sagara, Y. Rotaxane-Based Dual Function Mechanophores Exhibiting Reversible and Irreversible Responses. *J. Am. Chem. Soc.* **2021**, *143*, 9884−9892.
(82) Sagara, Y.; Traeger, H.; Li, J.; Okado, Y.; Schrettl, S.; Tamaoki, N.; Weder, C. Mechanically Responsive Luminescent Polymers Based on Supramolecular Cyclophane Mechanophores. *J. Am. Chem. Soc.* **2021**, *143*, 5519.
(83) Traeger, H.; Sagara, Y.; Kiebala, D. J.; Schrettl, S.; Weder, C. Folded Perylene Diimide Loops as Mechanoresponsive Motifs. *Angew. Chem., Int. Ed.* **2021**, *60*, 16191−16199.
(84) Freikamp, A.; Cost, A.-L.; Grashoff, C. The Piconewton Force Awakens: Quantifying Mechanics in Cells. *Trends in Cell Biol.* **2016**, *26*, 838−847.
(85) Liu, Y.; Galior, K.; Ma, V. P.-Y.; Salaita, K. Molecular Tension Probes for Imaging Forces at the Cell Surface. *Acc. Chem. Res.* **2017**, *50*, 2915−2924.
(86) Grashoff, C.; Hoffman, B. D.; Brenner, M. D.; Zhou, R.; Parsons, M.; Yang, M. T.; McLean, M. A.; Sligar, S. G.; Chen, C. S.; Ha, T.; Schwartz, M. A. Measuring mechanical tension across vinculin reveals regulation of focal adhesion dynamics. *Nature* **2010**, *466*, 263−267.
(87) Brockman, J. M; Blanchard, A. T; Pui-Yan, V.; Derricotte, W. D; Zhang, Y.; Fay, M. E; Lam, W. A; Evangelista, F. A; Mattheyses, A. L; Salaita, K. Mapping the 3D orientation of piconewton integrin traction forces. *Nat. Methods* **2018**, *15*, 115−118.
(88) Merindol, R.; Delechiave, G.; Heinen, L.; Catalani, L. H.; Walther, A. Modular Design of Programmable Mechanofluorescent DNA Hydrogels. *Nat. Commun.* **2019**, *10*, 528.
(89) Creusen, G.; Schmidt, R. S.; Walther, A. One-Component DNA Mechanoprobes for Facile Mechanosensing in Photopolymerized Hydrogels and Elastomers. *ACS Macro Lett.* **2021**, *10*, 671−678.
(90) Ogi, S.; Sugiyasu, K.; Takeuchi, M. Synthesis of a Doubly Strapped Light-Harvesting Porphyrin Bearing Energy Donor Molecules Hanging on to the Straps: An Attempt toward Macroscopic Control over Molecular Conformation That Affects the Efficiency of Fluorescence Resonance Energy Transfer. *Bull. Chem. Soc. Jpn.* **2011**, *84*, 40−48.
(91) Kotani, R.; Yokoyama, S.; Nobusue, S.; Yamaguchi, S.; Osuka, A.; Yabu, H.; Saito, S. Bridging pico-to-nanonewtons with a ratiometric force probe for monitoring nanoscale polymer physics before damage. *Nat. Commun.* **2022**, *13*, 303.
(92) Yuan, C.; Saito, S.; Camacho, C.; Irle, S.; Hisaki, I.; Yamaguchi, S. A π-Conjugated System with Flexibility and Rigidity That Shows Environment-Dependent RGB Luminescence. *J. Am. Chem. Soc.* **2013**, *135* (24), 8842−8845.
(93) Kotani, R.; Sotome, H.; Okajima, H.; Yokoyama, S.; Nakaike, Y.; Kashiwagi, A.; Mori, C.; Nakada, Y.; Yamaguchi, S.; Osuka, A.; Sakamoto, A.; Miyasaka, H.; Saito, S. Flapping Viscosity Probe That Shows Polarity-Independent Ratiometric Fluorescence. *J. Mater. Chem. C* **2017**, *5*, 5248−5256.
(94) Zhang, Z.; Wu, Y.-S.; Tang, K.-C.; Chen, C.-L.; Ho, J.-W.; Su, J.; Tian, H.; Chou, P.-T. Excited-State Conformational/Electronic Responses of Saddle-Shaped *N*,*N*′-Disubstituted-Dihydrodibenzo-[*a*,*c*]phenazines: Wide-Tuning Emission from Red to Deep Blue and White Light Combination. *J. Am. Chem. Soc.* **2015**, *137*, 8509−8520.
(95) Chen, W.; Chen, C.-L.; Zhang, Z.; Chen, Y.-A.; Chao, W.-C.; Su, J.; Tian, H.; Chou, P.-T. Snapshotting the Excited-State Planarization of Chemically Locked *N*,*N*′-Disubstituted Dihydrodibenzo[*a*,*c*]phenazines. *J. Am. Chem. Soc.* **2017**, *139*, 1636−1644.
(96) Humeniuk, H. V.; Rosspeintner, A.; Licari, G.; Kilin, V.; Bonacina, L.; Vauthey, E.; Sakai, N.; Matile, S. White-Fluorescent Dual-Emission Mechanosensitive Membrane Probes that Function by Bending Rather than Twisting. *Angew. Chem., Int. Ed.* **2018**, *57*, 10559.
(97) Zhang, Z.; Song, W.; Su, J.; Tian, H. Vibration-Induced Emission (VIE) of *N*,*N*′-Disubstituted-Dihydribenzo[*a*,*c*]phenazines: Fundamental Understanding and Emerging Applications. *Adv. Funct. Mater.* **2020**, *30*, 1902803.
(98) Yamakado, T.; Takahashi, S.; Watanabe, K.; Matsumoto, Y.; Osuka, A.; Saito, S. Conformational Planarization versus Singlet Fission: Distinct Excited-State Dynamics of Cyclooctatetraene-Fused Acene Dimers. *Angew. Chem., Int. Ed.* **2018**, *57*, 5438−5443.
(99) Yamakado, T.; Otsubo, K.; Osuka, A.; Saito, S. Compression of a Flapping Mechanophore Accompanied by Thermal Void Collapse in a Crystalline Phase. *J. Am. Chem. Soc.* **2018**, *140*, 6245−6248.
(100) Borissov, A.; Maurya, Y. K.; Moshniaha, L.; Wong, W.-S.; Żyła-Karwowska, M.; Stępień, M. Recent Advances in Heterocyclic Nanographenes and Other Polycyclic Heteroaromatic Compounds. *Chem. Rev.* **2022**, *122*, 565−788.
(101) Mateo-Alonso, A. Pyrene-fused pyrazaacenes: from small molecules to nanoribbons. *Chem. Soc. Rev.* **2014**, *43*, 6311−6324.
(102) Wu, Z.-H.; Sun, W.-J.; Tian, H.-H.; Yu, Z.-F.; Guo, R.-X.; Shao, X.; Zhang, H.-Li. 9,10-Imide-Pyrene-Fused Pyrazaacenes (IPPA) as N-Type Doping Materials for High-Performance Non-volatile Organic Field Effect Transistor Memory Devices. *Adv. Electron. Mater.* **2019**, *5*, 1800598.

https://doi.org/10.1021/jacs.1c12955
J. Am. Chem. Soc. 2022, 144, 2804−2815

(103) Suga, K.; Yamakado, T.; Saito, S. Nitrogen-Substitution in the Flapping Wings of Cyclooctatetraene-Fused Molecules. *Bull. Chem. Soc. Jpn.* **2021**, *94*, 1999−2002.
(104) Kimura, R.; Kuramochi, H.; Liu, P.; Yamakado, T.; Osuka, A.; Tahara, T.; Saito, S. Flapping Peryleneimide as a Fluorogenic Dye with High Photostability and Strong Visible-Light Absorption. *Angew. Chem., Int. Ed.* **2020**, *59*, 16430−16435.
(105) Goto, Y.; Omagari, S.; Sato, R.; Yamakado, T.; Achiwa, R.; Dey, N.; Suga, K.; Vacha, M.; Saito, S. Dynamic Polymer Free Volume Monitored by Single-Molecule Spectroscopy of a Dual Fluorescent Flapping Dopant. *J. Am. Chem. Soc.* **2021**, *143*, 14306−14313.
(106) Grabowski, Z. R.; Rotkiewicz, K.; Rettig, W. Structural Changes Accompanying Intramolecular Electron Transfer: Focus on Twisted Intramolecular Charge-Transfer States and Structures. *Chem. Rev.* **2003**, *103*, 3899−4032.
(107) Behera, S. K.; Park, S. Y.; Gierschner, J. Dual Emission: Classes, Mechanisms, and Conditions. *Angew. Chem., Int. Ed.* **2021**, *60*, 22624−22638.
(108) Stevens, B.; Ban, M. I. Spectrophotometric determination of enthalpies and entropies of photoassociation for dissolved aromatic hydrocarbons. *Trans. Faraday Soc.* **1964**, *60*, 1515−1523.
(109) Lippert, E. V. Spektroskopische Bestimmung des Dipolmomentes aromatischer Verbindungen im ersten angeregten Singulettzustand. *Z. Elektrochem.* **1957**, *61*, 962−975.
(110) Mataga, N.; Kaifu, Y.; Koizumi, M. Solvent Effects upon Fluorescence Spectra and the Dipolemoments of Excited Molecules. *Bull. Chem. Soc. Jpn.* **1956**, *29*, 465−470.
(111) Lee, C. K.; Diesendruck, C. E.; Lu, E.; Pickett, A. N.; May, P. A.; Moore, J. S.; Braun, P. V. Solvent Swelling Activation of a Mechanophore in a Polymer Network. *Macromolecules* **2014**, *47*, 2690−2694.
(112) Clough, J. M.; van der Gucht, J.; Sijbesma, R. P. Mechanoluminescent Imaging of Osmotic Stress-Induced Damage in a Galssy Polymer Network. *Macromolecules* **2017**, *50*, 2043−2053.
(113) Wang, L.; Zhou, W.; Tang, Q.; Yang, H.; Zhou, Q.; Zhang, X. Rhodamine-Functionalized Mechanochromic and Mechanofluorescent Hydrogels with enhanced Mechanoresponsive Sensitivity. *Polymers* **2018**, *10*, 994.
(114) Jayathilaka, P. B.; Molley, T. G.; Huang, Y.; Islam, M. S.; Buche, M. R.; Silberstein, M. N.; Kruzic, J. J.; Kilian, K. A. Force-mediated molecule release from double network hydrogels. *Chem. Commun.* **2021**, *57*, 8484−8487.
(115) Colom, A.; Derivery, E.; Soleimanpour, S.; Tomba, C.; Molin, M. D.; Sakai, N.; González-Gaitán, M.; Matile, S.; Roux, A. A fluorescent membrane tension probe. *Nat. Chem.* **2018**, *10*, 1118−1125.
(116) López-Andarias, J.; Straková, K.; Martinent, R.; Jiménez-Rojo, N.; Riezman, H.; Sakai, N.; Matile, S. Genetically Encoded Supramolecular Targeting of Fluorescent Membrane Tension Probes within Live Cells: Precisely Localized Controlled Release by External Chemical Stimulation. *JACS Au* **2021**, *1*, 221−232.
(117) Piazzolla, F.; Mercier, V.; Assies, L.; Sakai, N.; Roux, A.; Matile, S. Fluorescent Membrane Tension Probes for Early Endosomes. *Angew. Chem., Int. Ed.* **2021**, *60*, 12258−12263.

https://doi.org/10.1021/jacs.1c12955
J. Am. Chem. Soc. 2022, 144, 2804−2815